JOURNAL OF THERMOPLASTIC COMPOSITE MATERIALS

Original Article

Journal of Thermoplastic Composite Materials
1–22

DOI: 10.1177/0892705719895055
journals.sagepub.com/home/jtc
SAGE

Preparation of high-strength SEBS nanocomposites reinforced with halloysite nanotube: Effect of SEBS-*g*-MA compatibilizer

Nazlı Arman, Emre Tekay and Sinan Şen

Abstract

Poly(styrene-*b*-ethylene-*co*-butylene-*b*-styrene) (SEBS)/organophilic halloysite nanotube (Org-HNT) nanocomposites were prepared by solution mixing and then compression molded. Maleic anhydride grafted SEBS (SEBS-*g*-MA) was also used as a compatibilizer in preparation of SEBS/SEBS-*g*-MA/Org-HNT ternary nanocomposites. Surface morphologies and both static and dynamic mechanical analyses as well as thermal stabilities of the nanocomposites were carried out. Both the binary and ternary nanocomposites exhibited higher tensile moduli, tensile strength, and toughness values compared to neat SEBS. The elastic modulus was found to increase about 385% and 320% with addition of 3 and 5 phr Org-HNT into the SEBS matrix, respectively, while the maximum toughness was achieved via SEBS-5H composite with an increase of 45%. The ternary nanocomposite having 3 phr Org-HNT and 10 phr SEBS-*g*-MA (3H10SMA) gave about a 325% and 103% increase in the elastic modulus and toughness, respectively, together with a 75% increase in the tensile strength as the maximum value. This result was ascribed to interactions of the surface of the nanotubes with the maleic anhydride (MA) group of the compatibilizer. The same nanocomposite was also found to have two times higher dynamic storage modulus at 25°C than neat SEBS and almost the same damping value, which is an indication of improvement in the elastic character of SEBS without impairing its damping ability. Although a much higher damping value was obtained via use of 20 phr SEBS-*g*-MA with the same amount of nanotubes, the corresponding storage modulus decreased too much, close to that of neat SEBS. The enhanced tensile modulus, strength, and toughness of the 3H10SMA nanocomposite, which is consistent with its dynamic mechanical properties, indicate a good balance between the toughness/damping and

Department of Polymer Engineering, Yalova University, Yalova, Turkey

Corresponding author:
Sinan Şen, Department of Polymer Engineering, Yalova University, Yalova 77200, Turkey.
Email: sinans@yalova.edu.tr

stiffness. Moreover, all the nanocomposites exhibited better thermal stabilities than neat SEBS, showing higher midpoint degradation temperatures and peak maximum temperatures at which the maximum degradation occurs.

Keywords
SEBS, nanocomposites, tensile mechanical properties, dynamic mechanical analysis, SEBS-*g*-MA compatibilizer, halloysite nanotube

Introduction

The most commonly used polymers of the styrenic thermoplastic elastomer family are known to be poly(styrene-*b*-butadiene-*b*-styrene), poly(styrene-*b*-ethylene-*co*-butylene-*b*-styrene) (SEBS), and poly(styrene-*b*-isoprene-*b*-styrene).[1] Among them, SEBS is a styrenic thermoplastic elastomer with a saturated backbone and it has been widely used in the production of polymer blends and composites to increase the toughness and impact resistance of engineering plastics.[2] It has been utilized in different applications such as coatings, adhesives, footwear, impact modifiers for plastics,[1] as well as automotive parts and white goods.[3,4] SEBS and maleic anhydride-grafted SEBS (SEBS-*g*-MA) polymers have been studied in different researches as matrix and compatibilizer, respectively. The ST Lim research group prepared SEBS/organophilic montmorillonite (Org-MMT) nanocomposite by the solvent casting method in different compositions without the use of any compatibilizer to improve the thermal properties of neat SEBS copolymer.[5] The increase in thermal degradation temperature in the nanocomposites was found to be directly proportional to the amount of the clay. Ganguly et al. reported that MMT clay modified with dimethyl dehydrogenated tallow quaternary ammonium salt increased storage modulus of SEBS, whereas it decreased its damping factor.[6] In the same study, a much higher tensile strength and toughness in SEBS/MMT nanocomposites with use of 4 phr Org-MMT was achieved via melt intercalation process in comparison with the solution process. On the other hand, the tensile modulus was found to increase by solution process much more.

SEBS-*g*-MA is used as the compatibilizer in the preparation of polymeric–clay nanocomposites in order to improve both the polymer–clay interactions and the mechanical strength of the nanocomposite.[7–11] Mostafa Ranjbar et al. prepared polypropylene (PP)/Org-MMT nanocomposites with high strength and toughness, which were produced in the presence of SEBS-*g*-MA. They reported the formation of a balance between toughness and strength for the nanocomposites resulting from uses of the clay and the compatibilizer together in optimized compositions.[11] Wen-Chic Chen et al. produced SEBS/Org-MMT nanocomposite by the melt blending method.[12] The effects of two different compatibilizers, SEBS-*g*-MA and maleic anhydride grafted polypropylene (PP-*g*-MA), on the dispersion of the clay were investigated. The composites prepared by PP-*g*-MA showed a higher tensile modulus and tensile strength compared to those with SEBS-*g*-MA, even though SEBS-*g*-MA was found to be more effective in the exfoliation of clay in the SEBS matrix. The nanocomposite containing 7% Org-MMT

and 20% PP-*g*-MA showed a 196% improvement in tensile modulus compared to pure SEBS. The better enhancement via PP-*g*-MA compatibilizer was ascribed to the crystalline structure of PP-*g*-MA presenting more energy dissipation.[12,13] In another study, SEBS/layered clay nanocomposites using an internal mixer by melt blending method was prepared in the presence of SEBS-*g*-MA compatibilizer. The maximum elongation was observed in the composition with the SESB/SEBS-*g*-MA/MMT ratio of 80:20:10, while the maximum tensile strength value was reached in the 95:5:10 composition.[14] Thermal stability was enhanced more in SEBS/SEBS-*g*-MA/MMT composites in comparison with those having no compatibilizer. The decomposition temperature for the SEBS/SEBS-*g*-MA/MMT with a ratio of 90:10:10 was found to increase about 60°C compared to neat SEBS. Moreover, storage moduli of ternary nanocomposites were reported to be higher than that of SEBS/MMT binary composite in a broad range of temperatures.

Halloysite nanotubes (HNTs) are members of naturally occurring alumina silicate clay family and are expressed in closed formula as $Al_2Si_2O_5(OH)_4nH_2O$. They have the same chemical structure as kaolin clay and a similar geometry to carbon nanotubes. The outer diameter of the tubular HNTs varies between 30 nm and 90 nm and the inner diameter varies between 10 nm and 100 nm.[15] Many thermoplastics such as polyamide, polystyrene, PP, polyurethane, and polymethylmethacrylate as well as elastomers have been reinforced with small amounts of HNT clays by both melt blending and solution techniques.[16–18] MY Ong et al. produced PP/polyethylene (PE)/HNT nanocomposite using melt compounding technique and reported increase in the crystallization rate of PP/PE blends due to nucleation effect of the nanotubes.[17] In another study, HNTs were used for preparation of poly(ethylene-*co*-vinyl acetate-*co*-carbon monoxide) thermoplastic elastomer-based nanocomposite films via the solution casting method.[18] The high tensile strength and crystallinity were obtained with 1% HNT loading, whereas they decreased at higher loading percentages of the nanotubes. The decreases in the strength and crystallinity properties were attributed to nanotube aggregates and nonhomogeneous dispersion of the nanotubes in the matrix, as observed from their scanning electron microscope (SEM) images. Despite the wide use of HNT and maleated compatibilizers with different polymers in the production of nanocomposites, there has been no attempt so far to produce SEBS/HNT binary or ternary nanocomposites.

This article reports the production of novel SEBS/HNT and SEBS/SEBS-*g*-MA/HNT nanocomposites. It was aimed to show the effect of HNT clay on the improvement of weak mechanical strength of SEBS thermoplastic elastomer without impairing its toughness property. The HNT clay was modified with cetyltrimethyl ammonium bromide (CTAB) using the cryoscopic expansion/modification (C-XP/M) method[19] to obtain organophilic HNTs (Org-HNTs). The nanocomposites were prepared by solution mixing technique in a planetary (revolution/centrifugal rotation) type high-shear mixer.[20] The high-shear concentrated solution mixing technique was selected to decrease possible degradation of SEBS and SEBS-*g*-MA polymers encountered in melt-mixing.[19] The SEBS-*g*-MA compatibilizer was also used to improve the interaction between the nanotubes and SEBS polymer. The morphological, static, and dynamic mechanical properties as well as thermal properties of the SEBS/Org-HNT binary and

SEBS/SEBS-*g*-MA/Org-HNT ternary nanocomposites were examined in terms of degree of nanotube loading and compatibilizer.

Experimental

Materials

The SEBS block copolymer with a brand name of Taipol 6151 (viscosity: 1700 cP in 10 wt% toluene solution and at 25°C) was supplied by TSRC Corporation (Taipei, Taiwan). As-received SEBS contains 32 wt% styrene and a tiny amount of silica used as anticaking/antisticking agent. SEBS-*g*-MA block copolymer with a brand name of FG 1901X (melt flow index of 22 g/10 min, 230°C, 5 kg; viscosity: 1000 cP in 25 wt% toluene solution at 25°C) containing 30 wt% styrene and 1.84 wt% maleic anhydride was obtained from Kraton Corporation (Dover, Ohio, USA). HNT having a cation exchange capacity of 20 meq/100 was donated by the Esan Company (Istanbul, Turkey) and CTAB as the modification agent and tetrahydrofuran (THF) were purchased from Sigma-Aldrich (Steinheim, Germany).

Modification of HNTs by C-XP/M method

The nanotubes were modified via C-XP/M method[19]; 0.1 g CTAB calculated based on the cation exchange capacity of the HNT was dissolved in 40 mL deionized water at 50°C using a magnetic stirrer. Then, 2 g of HNT was added to the CTAB solution and stirred for 3 h. The solution was frozen at −20°C and the frozen solution was placed in the lyophilizer and sublimation of water was performed for 72 h. Finally, dry Org-HNT was obtained and stored in a desiccator.

Preparation of SEBS/Org-HNT and SEBS/SEBS-g-MA/Org-HNT nanocomposites by solution process

The nanocomposites were produced by dispersing Org-HNT in THF solvent (10 mL of THF per 1 g of solid mass) using a magnetic stirrer in a closed vessel and then dissolving SEBS-*g*-MA and SEBS polymers, respectively, in this solution, which was followed by evaporation of the solvent. In order to provide a more homogeneous mixture, the prepared composite solutions were mixed for 15 min at 1500 r min^{-1} with a planetary type high-speed mixer (KuraboMazerustar-KK250, Japan).[20] The homogeneous polymer–nanotube solutions were poured into Teflon molds and left in the fume hood for 8 h, then dried at 50°C for 2 h in a vacuum oven to remove THF completely. The component ratios in the composites were determined as phr based on the weight of the SEBS polymer matrix (Table 1). The resultant nanocomposites were compression molded with dimensions of 50 × 50 × 1 mm^3 using a hot press machine (Gülnar Makine, Turkey) at 200°C for 2 min of heating under 40 bar followed by 1.5 min of cooling under 80 bar.

Table 1. The compositions of SEBS/Org-HNT and SEBS/SEBS-*g*-MA/Org-HNT nanocomposites.

Material	SEBS (phr)	SEBS-*g*-MA (phr)	Org-HNT (phr)
SEBS	100	—	—
SEBS-1H	100	—	1
SEBS-3H	100	—	3
SEBS-5H	100	—	5
1H-10SMA	100	10	1
3H-10SMA	100	10	3
5H-10SMA	100	10	5
3H-5SMA	100	5	3
3H-10SMA	100	10	3
3H-20SMA	100	20	3

SEBS/Org-HNT: poly(styrene-*b*-ethylene-*co*-butylene-*b*-styrene)/organophilic halloysite nanotube; SEBS-*g*-MA/Org-HNT: poly(styrene-*b*-ethylene-*co*-butylene-*b*-styrene)/maleic anhydride grafted SEBS/organophilic halloysite nanotube; SMA: SEBS-*g*-MA.

Characterization

X-ray diffraction (XRD) analyses of HNT and Org-HNT clays were carried out using a Rigaku D/Max 2200 Ultimat diffractometer (Rigaku, Tokyo, Japan, with copper K_α radiation ($\lambda = 1.54$ Å) at 40 mA and 40 kV with a scanning rate of 2° min^{-1}. Thermogravimetric analyses (TGA) of the nanotubes and the nanocomposites were performed by Seiko TG/DTA 6300 (Seiko Instruments, Tokyo, Japan) under nitrogen atmosphere at 10°C min^{-1}. Morphological characterizations of nanotubes and cryo-fractured surfaces of neat SEBS and the composites were done by SEM (ESEM-FEG/EDAX Philips XL-30 microscope, Philips, Eindhoven, The Netherlands). The neat SEBS sample was cryofractured and then its surface was analyzed using the Element EDS system including the APEX standard software (EDS PV6500/00 SS) with EDAX Z2e analyzer attached to the instrument. The resultant semiquantitative data are given in the Supplementary Material File. Fourier-transform infrared (FTIR) analyses of the representative samples were done by a Perkin Elmer 1600 FTIR-ATR spectrophotometer (Waltham, Massachusetts, USA).

Tensile tests were carried out with a Zwick/Roell machine (Zwick GmbH & Co., KG, Germany) equipped with a 1 kN load cell. The test specimens with dimensions of 50 × 5.0 × 1.0 mm^3 were tested at room temperature with a drawing rate of 50 mm min^{-1}. Dynamic mechanical analysis (DMA) was carried out in a single cantilever bending mode using a TA Instruments analyzer (Q800, TA Instruments, New Castle, Delaware, USA) under a nitrogen atmosphere with a constant frequency (1 Hz) and at a heating rate of 10°C min^{-1}. The DMA analyses were performed with test specimens having dimensions of 50 × 8.0 × 1.0 mm^3.

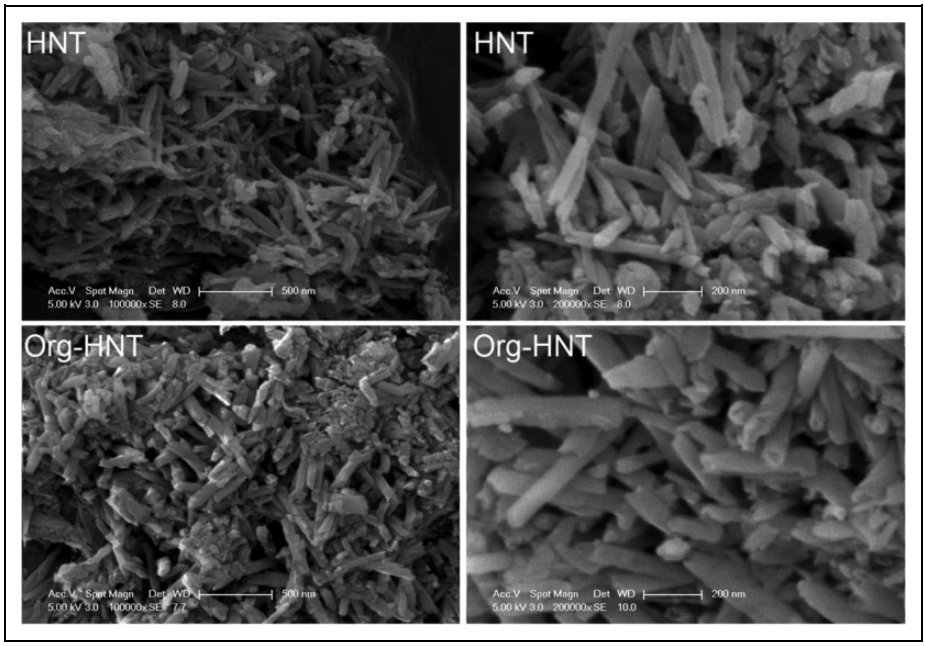

Figure 1. SEM images of HNT clays.
SEM: scanning electron microscope; HNT: halloysite nanotube.

Results and discussion

Characterization of HNT clays

SEM images of pure HNT and Org-HNT clays at different magnifications are given in Figure 1. When the SEM images are examined, pure HNTs in the form of aggregates were found to be relatively distant from each other and maintain their tubular structure. In addition, after the C-XP/M process, relative expansion of the nanotubes' volume and some deformations of tubes' ends were observed. These distortions may be caused by lyophilization process of the frozen solid water molecules and its replacement by CTAB molecules interacting with the silanol groups present at the ends of the HNTs.[19] As a result of surface modification, it was thought that HNTs with reduced intertubular interactions would exhibit better distribution in the polymer matrix and could establish better interactions with the matrix and compatibilizer.

TGA thermograms of pure HNT and Org-HNT clays and their derivative curves (DTG) are presented in Figure 2. Inorganic and polar HNTs have the potential to absorb moisture due to their nature and the weight loss up to 100°C on thermograms is due to the loss of moisture absorbed by the nanotubes. The weight loss of the Org-HNT in the range of 200–400°C is due to the degradation of the CTAB molecules attached to the nanotube surface. As a result of the analysis, the weight loss of CTAB molecules

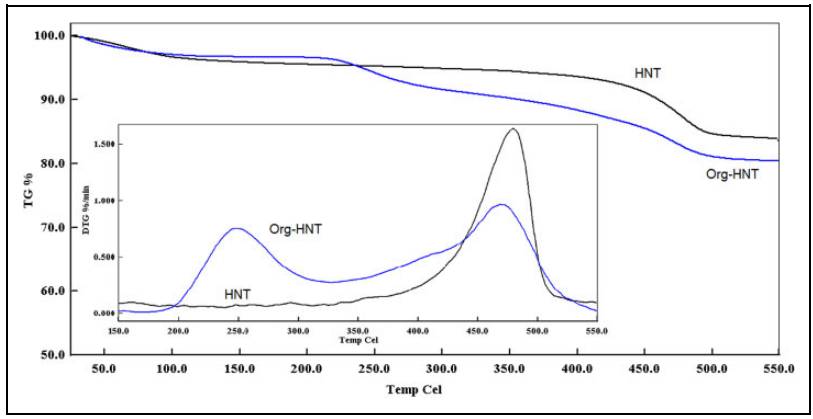

Figure 2. TGA thermograms of the HNT clays and their derivative curves.
TGA: thermogravimetric analysis; HNT: halloysite nanotube.

located on the surfaces of clay was determined as 5%. Weight loss in pure HNT and Org-HNT curves in the temperature range of 400–500°C is due to the removal of crystal water in the structure of the clay.[19] The DTG of Org-HNT nanotube (Figure 2, inset figure) indicates degradation of the CTAB molecule in the range of 200–320°C with a large peak, which is consistent with its thermogram. This result shows that the CTAB molecule interacts with the clay and the organophilic surface modification of clay is successfully performed.

The results of the XRD analyses are given in Figure S1 and Table S1 in the Supplementary Material File. There are three characteristic peaks of pure HNT at 2θ of 12.16°, 20.02°, and 24.48°[21] (Table S1, Supplementary Material File). The presence of these peaks in the XRD results of Org-HNT indicates that the tube geometry of HNTs is preserved after the surface modification. The Org-HNT was found to have an interlayer distance of 7.41 Å corresponding to the peak of $2\theta = 11.92°$ of the d_{001} basal plane. When the interlayer spacing of unmodified HNT of the same basal plane (7.27 Å) is compared, it is seen that the distance between the nanotube layers increases slightly after modification. This is thought to be due to CTAB molecules intercalating between the alumina silicate layers of the nanotube during the lyophilization process and separate the clay layers from each other.

Morphological characterization of SEBS elastomer

The SEM characterization of neat SEBS elastomer was found to include some spherical-shaped white particles (Figure S2, Supplementary Material File). Energy dispersive X-ray analysis (EDAX) of the whole area was done for the SEM image of SEBS elastomer at 1000× magnification and the silicon (Si) percentage was found to be approximately 0.74 (Figure S2, Supplementary Material File). In order to clarify the chemical structure of these white particles, some neat SEBS was burned at 600°C in

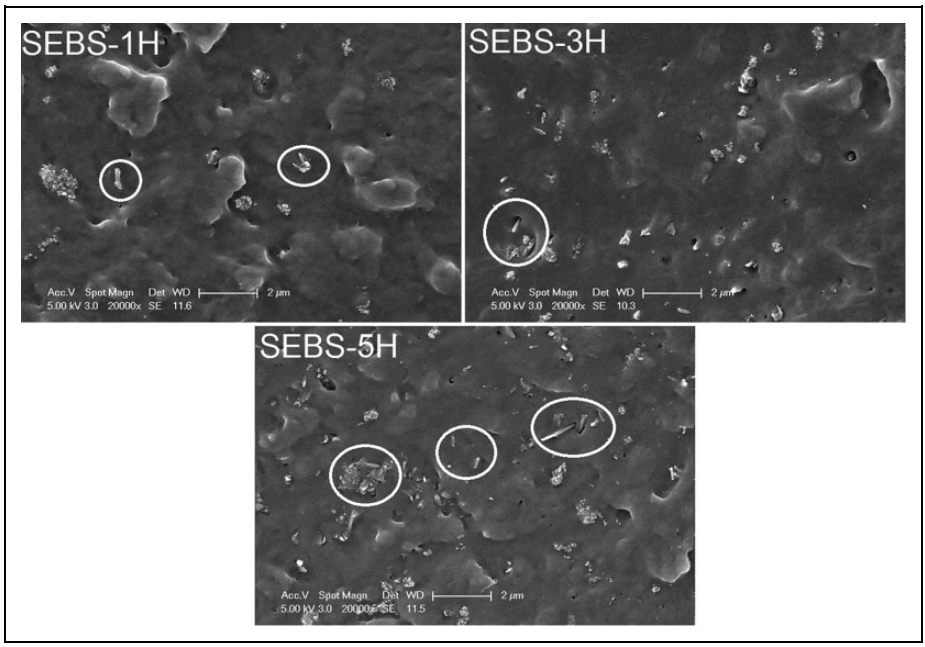

Figure 3. Low-magnification SEM images for cryofractured surfaces of SEBS/Org-HNT nanocomposites.
SEM: scanning electron microscope; SEBS/Org-HNT: poly(styrene-*b*-ethylene-*co*-butylene-*b*-styrene)/organophilic halloysite nanotube.

the muffle furnace and then SEM and EDAX of the white residue remaining from the combustion process were done (Figure S3, Supplementary Material File). As a result of the analysis, it is seen that atomic percentages of the Si and oxygen elements are very close to silicon dioxide (SiO_2) ratio. It is known that minor amounts of SiO_2 (silica) as anti-sticking/anticaking agent are added to SEBS elastomer and other styrenic elastomers, which are produced in high amounts, in order to prevent the particles from sticking to each other.[22] Based on the EDAX results and SEM images of SEBS elastomer, it was concluded that the white particles in Figure S2 and Figure S3 (Supplementary Material File) are silica fillers.

Morphological characterization of SEBS/Org-HNT and SEBS/SEBS-g-MA/Org-HNT nanocomposites

SEM images of the cryo-fractured surfaces of the composites are shown in Figures 3 to 6. The low- and high-magnification SEM images of binary nanocomposites containing only Org-HNT in different ratios (1, 3, and 5 phr) are given in Figures 3 and 4, respectively. As it can be seen from both the low- and high-magnification SEM images, SEBS-1 H and SEBS-3 H nanocomposites have a more homogeneous nanotube

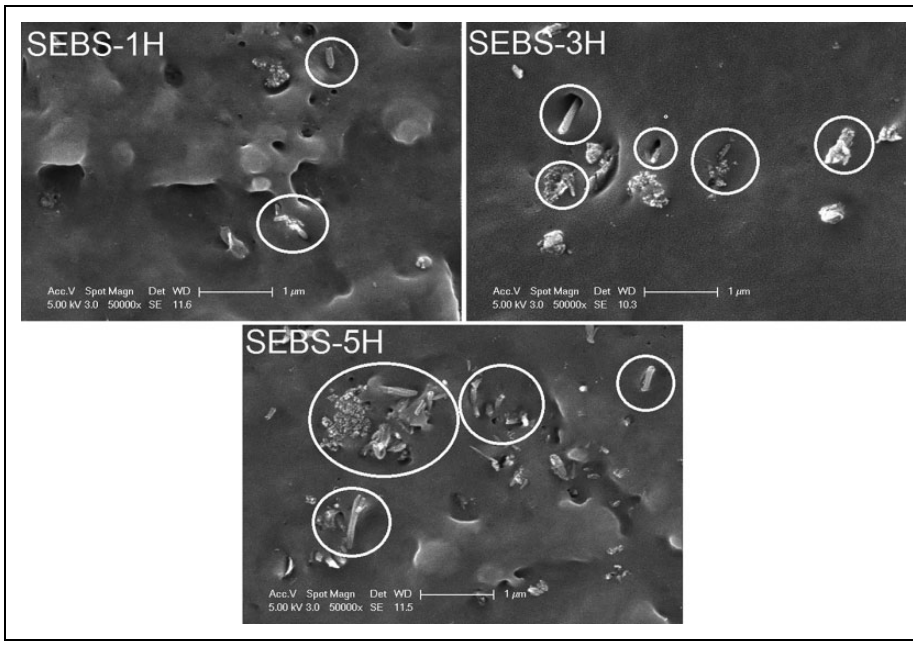

Figure 4. High-magnification SEM images for cryofractured surfaces of SEBS/Org-HNT nanocomposites.
SEM: scanning electron microscope; SEBS/Org-HNT: poly(styrene-*b*-ethylene-*co*-butylene-*b*-styrene)/organophilic halloysite nanotube.

dispersion compared to SEBS-5 H nanocomposite. In addition, the presence of the silica filler in the SEBS matrix, which is used as an anti-sticking agent, being partially around/on the nanotubes (Figure 4), may have contributed to the distribution of the nanotubes in the matrix. In this case, it can be said that a silica/HNT hybrid filler-reinforced composite structure having fillers with spherical and tubular geometry is formed. Relatively, a much smaller amount of silica may cause a synergistic effect with the HNT clay as a hybrid filler system[23] for a good dispersion of the nanotubes by decreasing their intertubular interactions. In the SEBS-5 H binary composite, as a result of increase in the HNT amount, the presence of aggregates formed by nanotubes were observed together with finely dispersed nanotubes ones. It is also clear from the high-magnification images (Figure 4) that pullout type toughness enhancing fracture mechanism is observed on the fractured surfaces.[23,24]

SEM images of fracture surfaces of ternary SEBS/SEBS-*g*-MA/Org-HNT nanocomposites with a constant compatibilizer amount (10 phr SMA) and varying Org-HNT loading degrees (1–3 phr) are given in Figure 5. Among these nanocomposites, it is seen that 1 and 3 phr Org-HNT loading exhibits good dispersion in the matrix with the use of SEBS-*g*-MA compatibilizer. Reducing the intertubular interactions of the nanotubes can be based on the hydrogen bond and dipole–dipole type interactions between the MA

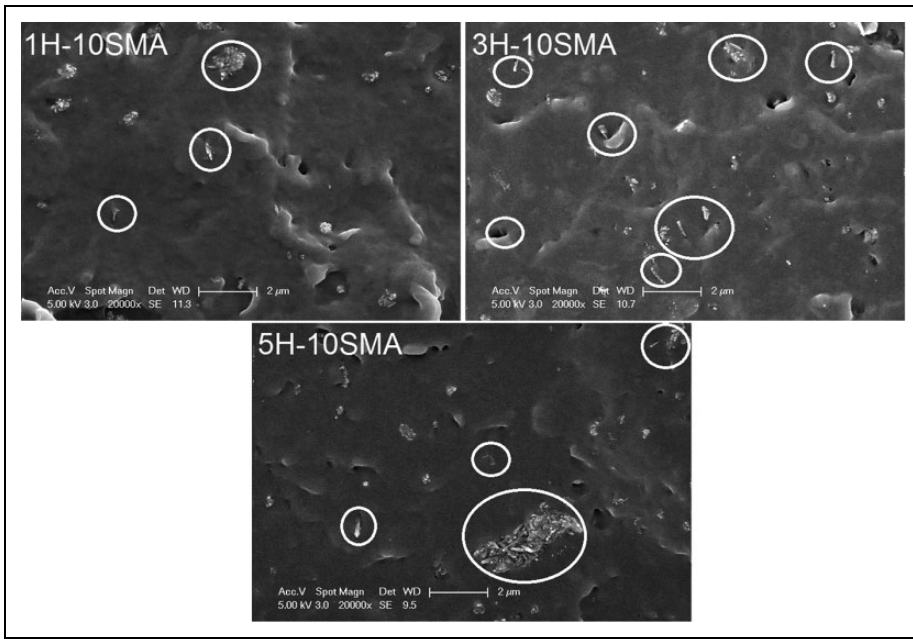

Figure 5. SEM images for cryofractured surfaces of SEBS/SEBS-*g*-MA/Org-HNT nanocomposites having 10 phr SEBS-*g*-MA and varying amounts of Org-HNT.
SEM: scanning electron microscope; SEBS/SEBS-*g*-MA/Org-HNT: poly(styrene-*b*-ethylene-*co*-butylene-*b*-styrene)/maleic anhydride grafted SEBS/organophilic halloysite nanotube; SEBS-*g*-MA: poly(styrene-*b*-ethylene-*co*-butylene-*b*-styrene)/maleic anhydride.

group of the compatibilizer and the surface of the nanotubes[24,25] as it was also confirmed with FTIR analyses (Figure 7). On the other hand, when 5 phr Org-HNT was used with the same amount of SEBS-*g*-MA, nanotube aggregates were observed (Figure 5), similar to the SEBS-5H binary nanocomposite (Figure 4). As a result, it can be said that the use of 10 phr SEBS-*g*-MA does not break intertubular interactions of the HNTs at this high degree of loading (5 phr Org-HNT).

Figure 6 shows SEM images of fractured surfaces of nanocomposites containing 3 phr Org-HNT and varying amounts of the compatibilizer. The nanocomposites 3H-5SMA and 3H-10SMA, having 5 and 10 phr compatibilizer, respectively, exhibit good nanotube dispersion. Interestingly, nanotube aggregates are formed in 3H-20SMA nanocomposite, although the amount of compatibilizer in this composite is relatively higher (Figure 6). This can be attributed to the use of a higher amount (20 phr) of SEBS-*g*-MA having a lower viscosity than the SEBS matrix polymer, resulting in a reduced solution/dispersion viscosity and relatively faster removal of THF during nanocomposite production, leading to nanotube aggregate formation.[26] It may also be probably due to less amount of THF molecules interacting with the Org-HNT to make it suspended in the solution in the presence of a high amount of SEBS-*g*-MA molecule.

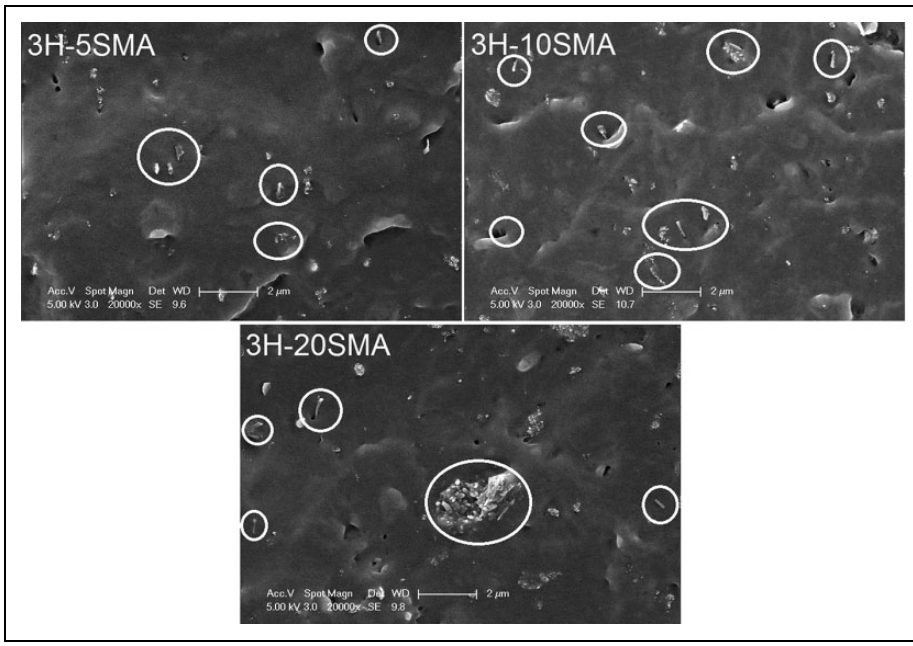

Figure 6. SEM images for cryofractured surfaces of SEBS/SEBS-*g*-MA/Org-HNT nanocomposites having 3 phr Org-HNT and different amounts of the compatibilizer.
SEM: scanning electron microscope; SEBS: poly(styrene-*b*-ethylene-*co*-butylene-*b*-styrene); SEBS/SEBS-*g*-MA/Org-HNT: poly(styrene-*b*-ethylene-*co*-butylene-*b*-styrene)/maleic anhydride grafted SEBS/organophilic halloysite nanotube.

FTIR analyses

FTIR spectra of Org-HNT and 3H-10SMA as representative composites are shown in Figure 7. In the spectrum of Org-HNT, the FTIR bands at 1469 and 2851 and 2921 cm^{-1} are related to C-H scissoring and C–H stretching vibrations, respectively, due to organic modifier of HNT clay. The peaks of HNT appearing at 3624 and 3692 cm^{-1} and 1643 $cm^{-1}$are assigned to O–H stretching of inner hydroxyl groups and O–H deformation of water, respectively.[20,27] In the spectrum of Org-HNT, the peaks at 999 and 1117 cm^{-1} and 905 $cm^{-1}$are assigned to Si-O stretching (outer siloxane groups) bands and Al-OH (inner/edge hydroxyl groups) bending vibrations, respectively.[20,28] From the FTIR spectrum of the 3H-10SMA, the peaks at 1117, 999, and 905 cm^{-1} were found to shift to 1068, 1028, and 907 cm^{-1}, respectively. These shifts have been attributed to hydrogen bonding interaction between the outer Si–O groups of HNT or its Al-OH and MA groups of the SEBS-*g*-MA polymer.[20,29] Particularly, the larger redshift observed in the Si–O stretching peak shows better interfacial interactions occurring between the outer surface of the HNT clay having silanol/siloxane groups and MA group of the SEBS-*g*-MA polymer. The much smaller shift in the Al-OH absorption peak, on the

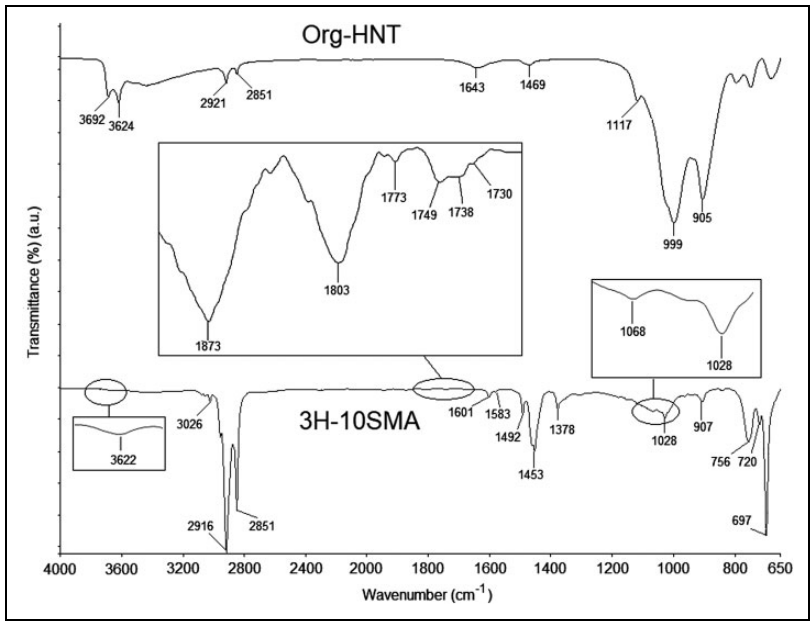

Figure 7. FTIR spectra of Org-HNT and 3H-10SMA nanocomposite.
FTIR: Fourier-transform infrared; Org-HNT: organophilic halloysite nanotube.

other hand, can be due to difficulty for interaction of the aluminol groups inside the lumen of the nanotubes via the MA group of SEBS-*g*-MA.[28,30] The peaks observed at 1873 and 1803 cm^{-1} can be assigned to C=O stretching vibration. The disappearance of absorption peak of C=O symmetric stretching (at 1704 cm^{-1}; Figure S4, Supplementary Material File) and appearance of new peaks at 1730, 1738, 1749, and 1773 cm^{-1} can be related to formation of ester bond between the HNT surface and MA group of the SEBS-*g*-MA.[20] Moreover, the peaks at 1492 and 1453 cm^{-1} are due to C=C stretching of aromatic benzene ring of SEBS.[31]

Tensile mechanical properties

The tensile test results of neat SEBS and the nanocomposites are given in Table 2. The elastic modulus, tensile strength, and toughness of the prepared SEBS/Org-HNT binary nanocomposites were found to be higher compared to pure SEBS. The increase in the modulus can be attributed to the use of high-modulus HNT clay acting as a reinforcing agent for the matrix.[8,19] The maximum elastic modulus value was obtained in SEBS-3H composite with an increase of approximately 385%, while the maximum toughness value was obtained in SEBS-5H composite with an increase of 45%. The elastic modulus and strength values were found to be more improved in SEBS-3H, compared to SEBS-5H due to the fact that the nanotubes are more homogeneously dispersed in the matrix

Table 2. Tensile mechanical properties of SEBS, SEBS/Org-HNT, and SEBS/SEBS-*g*-MA/Org-HNT nanocomposites.

Material	Elastic modulus, *E* (MPa)	Tensile strength (MPa)	Elongation at break (%)	Toughness (Nmm)
SEBS	9.99 ± 0.86	9.76 ± 0.31	597.30 ± 30.96	4110.65 ± 201.48
SEBS-1H	42.71 ± 1.78	8.28 ± 1.11	606.80 ± 29.73	4237.59 ± 148.25
SEBS-3H	48.64 ± 2.54	10.30 ± 1.10	676.97 ± 30.47	5119.78 ± 188.62
SEBS-5H	42.16 ± 2.19	11.48 ± 0.13	709.13 ± 23.17	6011.78 ± 111.18
1H-10SMA	38.49 ± 3.00	13.61 ± 0.82	721.46 ± 22.28	6945.10 ± 216.29
3H-10SMA	42.32 ± 2.98	17.10 ± 0.69	764.11 ± 23.55	8368.68 ± 221.64
5H-10SMA	40.60 ± 2.87	12.41 ± 0.27	691.83 ± 24.58	5831.15 ± 162.31
3H-5SMA	47.88 ± 7.32	14.16 ± 0.56	637.81 ± 1.12	6445.93 ± 161.49
3H-10SMA	42.32 ± 2.98	17.10 ± 0.69	764.11 ± 23.55	8368.68 ± 221.64
3H-20SMA	30.29 ± 0.40	16.19 ± 0.32	779.15 ± 17.47	9007.66 ± 119.43

SEBS: poly(styrene-*b*-ethylene-*co*-butylene-*b*-styrene); Org-HNT: organophilic halloysite nanotube; SEBS-*g*-MA/Org-HNT: poly(styrene-*b*-ethylene-*co*-butylene-*b*-styrene)/maleic anhydride grafted SEBS/organophilic halloysite nanotube; SMA: SEBS-*g*-MA.

(Figures 3 and 4), reinforcing the SEBS matrix more effectively. Moreover, the pullout of nanotubes from the polymer matrix observed from the surface of the cryofractured sample (Figure 4) may have contributed to the absorption of extra energy during tensile fracture. While the toughness value increased proportionally with the amount of clay, the elastic modulus value did not improve in the same way. The modulus of SEBS-5H composite showed a lower value than that of the SEBS-3H composite. This may be due to more homogeneous dispersion of the nanotubes in the matrix in SEBS-3 H and the presence of HNT aggregates in the SEBS-5 H, as shown in Figure 4. It can be said that the toughness–stiffness balance is established in the SEBS-3H nanocomposite among binary composites.

Table 2 also indicates the tensile test results of SEBS/SEBS-*g*-MA/Org-HNT ternary nanocomposites containing a constant amount of SEBS-*g*-MA (10 phr) with varying amounts of the clay (1, 3, and 5 phr). It is seen from the table that the tensile mechanical properties of all the ternary nanocomposites are improved compared to pure SEBS. On the other hand, their elastic modulus values were found to be lower than those of their binary counterparts (Table 2). This may be due to the use of SEBS-*g*-MA having a lower viscosity and lower styrene content as well as increased SEBS/Org-HNT ratio. The highest tensile strength, elongation at break, and toughness values were obtained for 3H-10SMA nanocomposite among those having 10 phr SEBS-*g*-MA. Compared to neat SEBS, this composition resulted in approximately a 75% increase in tensile strength, 28% increase in tensile elongation, and 103% increase in toughness. This can be due to the homogeneous dispersion of the Org-HNTs in the matrix (Figure 5) with the help

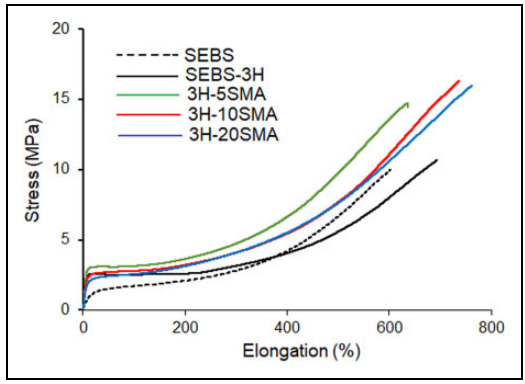

Figure 8. Stress–strain curves of neat SEBS and SEBS nanocomposites having 3 phr Org-HNT clay.
SEBS: poly(styrene-*b*-ethylene-*co*-butylene-*b*-styrene); Org-HNT: organophilic halloysite nanotube.

of their interactions with polar maleic anhydride on the compatibilizer (Figure 7), reinforcing the polymer matrix at the highest level. On the other hand, mechanical strength and toughness values of 5H-10SMA composite having higher amount of Org-HNT were found to be lower than the 3H-10SMA nanocomposite. This result can be based on the presence of large HNT aggregates (Figure 5) and the decrease in SEBS/Org-HNT ratio in the 5H-10SMA nanocomposite.

The 3 phr Org-HNT was selected as the optimum clay loading degree and the nanocomposites containing different ratios of SEBS-*g*-MA were prepared in order to investigate the effect of the amount of the compatibilizer on the properties by keeping the clay amount constant. Tensile stress–strain curves and mechanical test results of these nanocomposites with different amounts of the compatibilizer and constant nanotube ratio (3 phr Org-HNT) are given in Figure 8 and Table 2, respectively. Elastic modulus, tensile strength, elongation, and toughness values of all the nanocomposites containing different amounts of compatibilizers were found to be higher compared to pure SEBS. When the elastic modulus values were compared, the highest value was obtained for 3H-5SMA composite and the lowest value was obtained for 3H-20SMA composite. This may be due to presence of the SEBS-*g*-MA compatibilizer, which has lower viscosity and styrene content compared to SEBS. Although 3H-20SMA nanocomposite had the highest toughness and elongation values, the modulus and tensile strength values of this composite were lower than 3H-10SMA composite because it contains a higher amount of the compatibilizer. The decrease in the mechanical strength and modulus observed for 3H-20SMA may also be attributed to the presence of large nanotube aggregates in the same composite (Figure 6).

The tensile test results show that the mechanical properties of the SEBS thermoplastic elastomer can be improved using only the Org-HNT reinforcer (SEBS/Org-HNT). Moreover, they can be further enhanced with the use of Org-HNT/SEBS-*g*-MA dual components together with SEBS matrix.

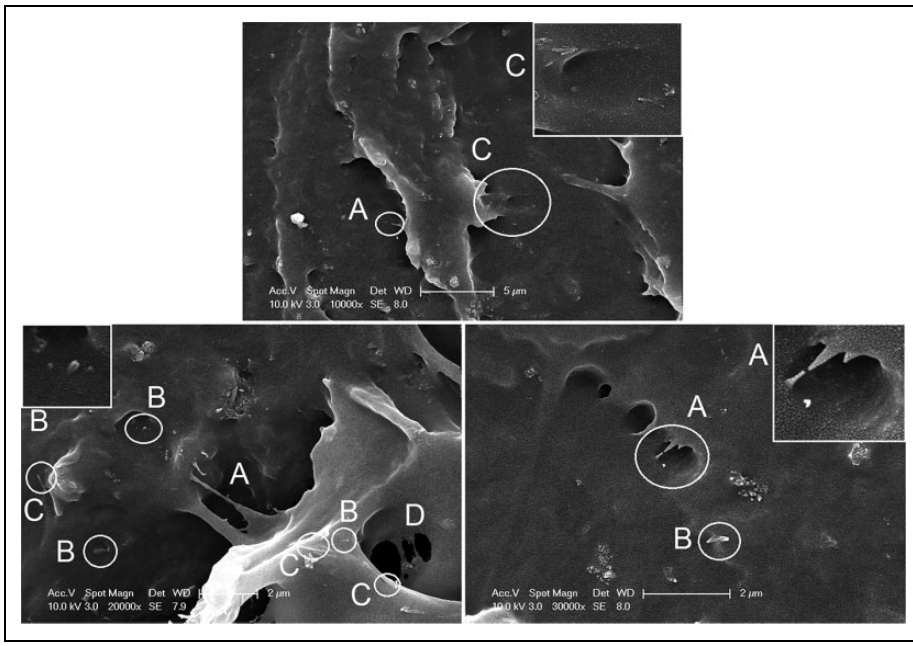

Figure 9. SEM images for the tensile fractured surfaces of 3H-10SMA nanocomposite exhibiting toughness-enhancing fracture mechanisms: A: crack-bridging; B: nanotube pullout; C: nanotubes dispersed in the matrix; and D: crazing.
SEM: scanning electron microscope.

SEM images of the tensile test fractured surface of the 3H-10SMA as a representative nanocomposite at different magnifications are given in Figure 9. As it can be seen from the figure, the nanocomposite exhibited toughness-enhancing fracture mechanisms like crack-bridging and nanotube pullout together with matrix crazing and nanotubes coated with matrix,[24,25] supporting the tensile toughness data of the composite (Table 2).

Dynamic mechanical properties

The dynamic mechanical properties of neat SEBS and the nanocomposites containing 3 phr Org-HNT were investigated by DMA as a function of the temperature. Table 3 shows the results of the analyses and, Figures 10 and 11 give the damping parameter (tan δ) versus temperature and storage modulus (E') versus temperature graphs, respectively. The tan δ values of the composites at the glass transition region of the ethylene–butylene (EB) segment, which is the soft block of SEBS thermoplastic elastomer, were lower compared to pure SEBS (Table 3). This may be due to the reinforcing effect of Org-HNT clay for the EB segments, thereby limiting their chain movements and reducing the damping ability.[32,33] This result is also in good accordance with increase in storage moduli of the nanocomposites at low temperatures compared to neat SEBS (Figure 11).

Table 3. Dynamic mechanical properties of neat SEBS and SEBS nanocomposites reinforced with 3 phr Org-HNT.[a]

Material	$\acute{E}_{-50^\circ C}$ MPa	$T_{gEB,}$ °C (tan δ_{max})	$\acute{E}_{25^\circ C}$ MPa	Tan $\delta_{25^\circ C}$	$\acute{E}_{90^\circ C}$ MPa	$T_{gPS,}$ °C (tan δ_{max})
SEBS	554.1	−50.00 (0.35)	56.23	0.037	19.81	90.00 (0.11)
SEBS-3H	534.3	−52.91 (0.26)	119.30	0.029	35.10	87.07 (0.20)
3H-5SMA	569.8	−53.93 (0.25)	148.70	0.023	36.87	88.04 (0.17)
3H-10SMA	663.2	−50.41 (0.27)	104.70	0.035	21.86	85.65 (0.25)
3H-20SMA	658.5	−51.08 (0.28)	63.45	0.048	43.26	69.37 (0.19)

SEBS: poly(styrene-*b*-ethylene-*co*-butylene-*b*-styrene); Org-HNT: organophilic halloysite nanotube; SMA: SEBS-*g*-MA.

[a]T_{gEB} and T_{gPS} are dynamic glass transition temperatures of ethylene–butylene (EB) and polystyrene (PS) blocks, respectively, which corresponds to their tan δ peak maximum (damping) values given in parentheses.

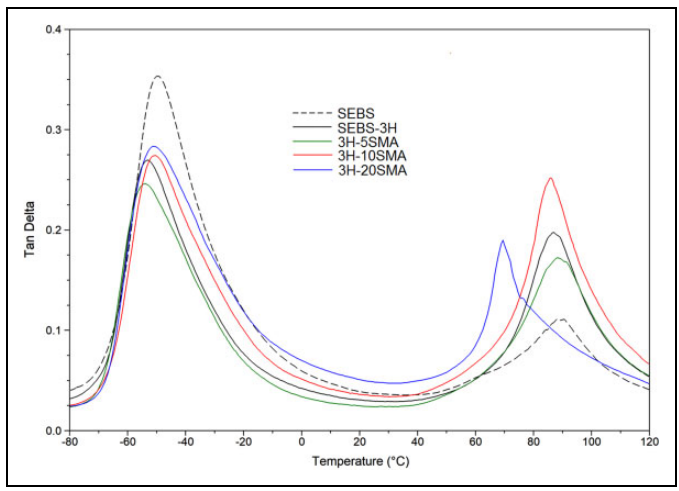

Figure 10. Tan δ versus temperature curves of neat SEBS and SEBS nanocomposites having 3 phr Org-HNT clay.
SEBS: poly(styrene-*b*-ethylene-*co*-butylene-*b*-styrene); Org-HNT: organophilic halloysite nanotube.

Moreover, the shift of tan δ peak maximum values of nanocomposites at this region to lower temperatures may result from the frictions between the nanotubes and the EB molecules passing through the rubbery phase. This may cause the earlier movements of the EB molecules close to the nanotubes.[34] The storage modulus value of the SEBS-3H binary composite at the low temperature region was found to be lower than neat SEBS, whereas all the composites containing the SEBS-*g*-MA compatibilizer have higher storage modulus values than the pure SEBS and SEBS-3H binary composite (Table 3). This is due to enhanced interactions between the nanotubes and the matrix and the

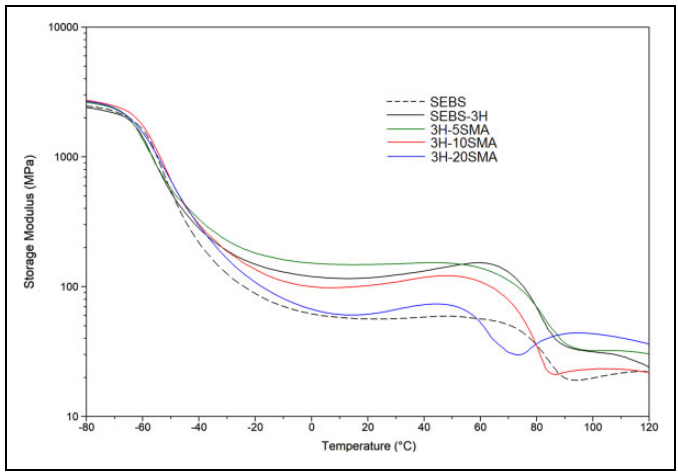

Figure 11. Storage modulus versus temperature curves of neat SEBS and SEBS nanocomposites having 3 phr Org-HNT clay.
SEBS: poly(styrene-*b*-ethylene-*co*-butylene-*b*-styrene); Org-HNT: organophilic halloysite nanotube.

development of the nanotube dispersion via compatibilizing effect of SEBS-*g*-MA. It can be said that possible hydrogen bonding and dipole–dipole interactions of the MA group of the compatibilizer with nanotube surface (Figure 7) increased the modulus value.[23,29] Among the ternary nanocomposites, 3H-10SMA and 3H-20SMA were found to have relatively broader damping temperature ranges and the highest tan δ at low temperatures (Figure 10). The former showed higher storage modulus and dynamic T_g at the low temperature region among all the composites (Figure 11).

In the glass transition region of the polystyrene (PS) block, all the nanocomposites exhibited higher damping values than pure SEBS (Table 3). This can be attributed to high amount of frictions between the nanotubes and polymer molecules. The frictions between the silica nanotubes and those due to more interactions between polymer molecules, since the PS block passes to the rubbery phase at this region, result in the damping of mechanical energy into heat.[34,35] The decrease in the dynamic glass transition temperature of the PS phase (Table 3) can also be explained by tan δ peak in the composites starting to rise at lower temperatures due to high degree of the abovementioned frictions. Moreover, the damping temperature range in this region is wider in all the composites than that of neat SEBS (Figure 10), indicating that the composites shows good damper performance.

The storage moduli of the composites at 25°C except that of 3H-20SMA were found to be approximately two times higher than neat SEBS (Table 3 and Figure 11). The increased storage moduli of the nanocomposites at 25°C are in agreement with the elastic moduli values obtained from static tensile test (Table 2). The elastic character of the material seems to be improved by the reinforcement of the polymer matrix by the Org-HNT clay. Although the damping values in this region decreases slightly in the SEBS-3H and 3H-5SMA composites compared to pure SEBS, it has a maximum value for the 3H-

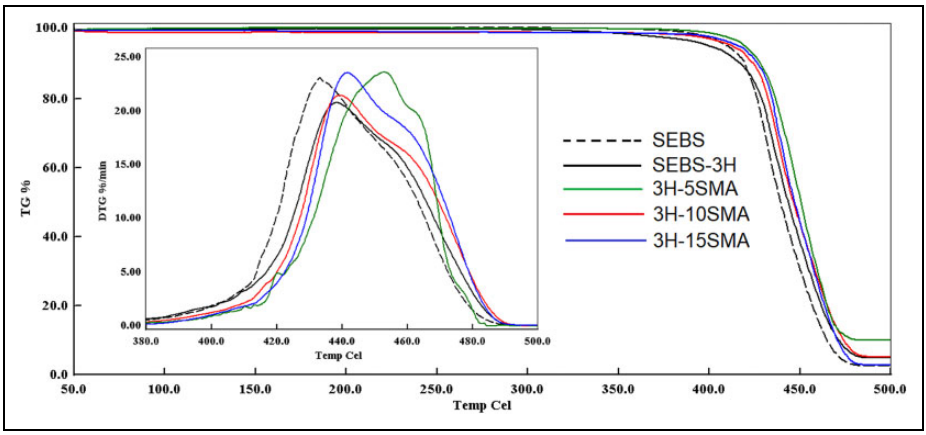

Figure 12. TGA thermograms of neat SEBS and SEBS nanocomposites having 3 phr Org-HNT clay and their derivative curves (inset figure).
TGA: thermogravimetric analysis; SEBS: poly(styrene-*b*-ethylene-*co*-butylene-*b*-styrene); Org-HNT: organophilic halloysite nanotube.

20SMA composite (Figure 10 and Table 3). The increase in damping value can be attributed to the relatively increased SEBS-*g*-MA ratio in 3H-20SMA with a higher amount of EB phase, which is also in agreement with its lowest storage modulus (Figure 11 and Table 3). For the 3H-10SMA nanocomposite, the damping value at 25°C is almost the same as that of neat SEBS (Table 3 and Figure 10) and its storage modulus value is much higher than that of pure SEBS and the 3H-20SMA composite. This result is quite remarkable that the increase in the modulus value together with the damping property of SEBS elastomer was achieved.

As a conclusion of dynamic and static mechanical analyses, it can be said that the optimum composite which provides the hardness–toughness balance is the 3H-10SMA nanocomposite.

TGA of the composites

TGA thermograms of neat SEBS and SEBS/Org-HNT and SEBS/SEBS-*g*-MA/Org-HNT nanocomposites containing 3 phr Org-HNT and their derivative thermograms and are shown in Figure 12. Table 4 shows the results of the TGA analyses. The initial degradation temperature (Td_{10}) at which the SEBS-3 H nanocomposite loses 10 wt% was found to be slightly lower than that of neat SEBS. This may be due to the catalytic effect of nanotubes in thermal decomposition of aliphatic polymer molecules.[36] On the other hand, the temperature (T_{d50}) at which 50% weight loss occurs and the temperature at maximum degradation rate were found be increased with the same composite having a lower decomposition rate (Table 4). This result can be ascribed to retarded weight loss due to the inhibition of volatile degradation products by the nanotube.[37]

Table 4. TGA data of neat SEBS and SEBS nanocomposites reinforced with 3 phr Org-HNT.

Material	T_{d10} (°C)	T_{d50} (°C)	Residue (%) at 500°C	Max. deg. rate (% min^{-1}) (peak max. temperature, °C)
SEBS	419.7	439.0	2.8	23.0 (433.2)
SEBS-*g*-MA	412.2	439.2	1.1	20.8 (441.5)
SEBS-3H	416.0	443.3	5.2	20.8 (438.0)
3H-5SMA	428.6	450.6	10.7	23.6 (452.7)
3H-10SMA	424.2	446.2	5.5	21.4 (439.1)
3H-20SMA	427.2	446.8	2.8	23.5 (441.5)

TGA: thermogravimetric; SEBS: poly(styrene-*b*-ethylene-*co*-butylene-*b*-styrene); Org-HNT: organophilic halloysite nanotube; SEBS-*g*-MA: maleic anhydride grafted SEBS; SMA: SEBS-*g*-MA.

On the other hand, all of the nanocomposites containing SEBS-*g*-MA compatibilizer have higher values of Td_{10}, Td_{50}, residue, and the maximum degradation temperature than neat SEBS and SEBS-3H binary composite. It can be explained by the synergistic effect caused by SEBS-*g*-MA and well-dispersed nanotubes with the help of the compatibilizer and so more volatile products trapped in their lumens. Moreover, higher peak maximum temperature and lower degradation rate of the SEBS-*g*-MA in comparison with that of neat SEBS (Figure S5, Supplementary Material File) may cause the nanocomposites having the compatibilizer to be more thermally stable than both SEBS and SEBS-3H binary nanocomposite.

Conclusion

SEBS/Org-HNT binary and SEBS/SEBS-*g*-MA/Org-HNT ternary nanocomposites were successfully prepared by solution mixing method. The morphological and mechanical properties of the composites were found to be dependent on both nanotube loading degree and presence of compatibilizer. From SEM analyses, a homogeneous nanotube dispersion was observed in SEBS binary composites containing 1 and 3 phr Org-HNT, while nanotube aggregates were observed with use of 5 phr Org-HNT. When 5 and 10 phr SEBS-*g*-MA was used in nanocomposites with constant HNT loading degree (3 phr), the nanotubes showed a homogeneous dispersion in the SEBS matrix as revealed by the SEM micrographs. However, nanotube aggregates formed by the use of 20 phr low-viscosity compatibilizer were most probably due to rapid evaporation of the solvent resulting from the decrease in solution viscosity. Thermal stabilities of the nanocomposites were also found to be higher than that of neat SEBS, indicating the thermal barrier effect of the nanotubes dispersed in the matrix. The T_{d10}, T_{d50}, residue amount, and maximum degradation temperature values increased in SEBS-*g*-MA containing nanocomposites compared to pure SEBS and SEBS/Org-HNT binary nanocomposites. Both the binary and ternary nanocomposites showed greater values of tensile moduli, tensile strength, and toughness compared to pure SEBS. The

SEBS/SEBS-*g*-MA/Org-HNT ternary nanocomposite having 3% Org-HNT and 10% SEBS-*g*-MA as an optimized composition displayed 325% and 103% increase in the elastic modulus and the toughness, respectively, The same composition also showed about 75% increase in the tensile strength as the maximum value, compared to neat SEBS. These results were attributed to interactions of the MA group of SEBS-*g*-MA and nanotubes' surfaces resulting in better dispersion of them in the matrix. The same nanocomposite also showed almost two times higher storage modulus at 25°C than neat SEBS with almost the same damping as neat SEBS. At a higher amount of SEBS-*g*-MA, higher damping with lower modulus was achieved. In conclusion, the SEBS-*g*-MA showed a beneficial effect as a compatibilizer between Org-HNT and SEBS matrix by improving the elastic character of SEBS without impairing its damping ability. This is accepted as a good indication of balanced stiffness and toughness/damping.

Funding

The author(s) disclosed receipt of the following financial support for the research, authorship, and/or publication of this article: The support given by Scientific Research Projects Coordination Department of Yalova University (project no. 2018/YL/0012) is gratefully acknowledged.

ORCID iD

Sinan Şen https://orcid.org/0000-0001-8062-8575

Supplemental material

Supplemental material for this article is available online.

References

1. Holden G and Legge N. *Styrenic thermoplastic elastomers*. New York: Thermoplastic elastomer'HanserPublisers, 1996.
2. de Oliveira CIR, Rocha MCG, de Assis JT, et al. Morphological, mechanical, and thermal properties of PP/SEBS/talc composites. *J Thermoplast Compos Mater* 2019: DOI: 10.1177/0892705719876678.
3. Li X, Yang J, Zhou X, et al. Effect of compatibilizer on morphology, rheology and properties of SEBS/clay nanocomposites. *Polym Test* 2018; 67: 435–440.
4. Lai SM and Chen CM. Preparation, structure, and properties of styrene–ethylene–butylene–styrene block copolymer/clay nanocomposites: part III. Effectiveness of compatibilizers. *Eur Polym J* 2007; 43: 2254–2264.
5. Lim S, Lee C, Kwon Y, et al. Polystyrene-b-poly (Ethylene-r-butylene)-b-polystyrene triblock copolymer/organoclay nanocomposites and their phase characteristics. *JMacromol SciB* 2004; 43: 577–589.
6. Ganguly A, De Sarkar M and Bhowmick AK. Thermoplastic elastomeric nanocomposites from poly [styrene–(ethylene-co-butylene)–styrene] triblock copolymer and clay: preparation and characterization. *J Appl Polym Sci* 2006; 100: 2040–2052.
7. Du M, Guo B and Jia D. Thermal stability and flame retardant effects of halloysite nanotubes on poly (propylene). *Eur Polym J* 2006; 42: 1362–1369.

8. Jia ZX, Luo YF, Yang SY, et al. Morphology, interfacial interaction and properties of styrene-butadiene rubber/modified halloysite nanotube nanocomposites. *Chin J Polym Sci* 2009; 27: 857–864.
9. Kamble R, Ghag M, Gaikawad S, et al. Halloysite nanotubes and applications: a review. *J Adv Sci Res* 2012; 3:25–29.
10. Saheb SM, Tambe P and Malathi M. Influence of halloysite nanotubes and intumescent flame retardant on mechanical and thermal properties of 80/20 (wt/wt) PP/ABS blend and their composites in the presence of dual compatibilizer. *J Thermoplast Compos Mater* 2018; 31: 202–222.
11. Ranjbar M, Arefazar A and Bakhshandeh G. Constituting balance between strength and toughness in nanocomposites based on PP/SEBS-g-MA blends. *J Thermoplast Compos Mater* 2014; 27: 1589–1606.
12. Chen WC, Lai SM and Chen CM. Preparation and properties of styrene–ethylene–butylene–styrene block copolymer/clay nanocomposites: I. Effect of clay content and compatibilizer types. *Polym Int* 2008; 57: 515–522.
13. Százdi L, Pukánszky Jr B, Vancso GJ, et al. Quantitative estimation of the reinforcing effect of layered silicates in PP nanocomposites. *Polymer* 2006; 47: 4638–4648.
14. Chang YW, Shin JY and Ryu SH. Preparation and properties of styrene–ethylene/butylene–styrene (SEBS)–clay hybrids. *Polym Int* 2004; 53: 1047–1051.
15. Kausar A. Review on polymer/halloysite nanotube nanocomposite. *Polym Plast Tech Eng* 2018; 57: 548–564.
16. Beatrice CA, Branciforti MC, Alves RM, et al. Rheological, mechanical, optical, and transport properties of blown films of polyamide 6/residual monomer/montmorillonite nanocomposites. *J Appl Polym Sci* 2010; 116: 3581–3592.
17. Ong M and Chow W. Kinetics of crystallization for polypropylene/polyethylene/halloysite nanotube nanocomposites. *J Thermoplast Compos Mater* 2018.DOI: 0892705718807953.
18. George G, Selvakumar M, Mahendran A, et al. Structure–property relationship of halloysite nanotubes/ethylene–vinyl acetate–carbon monoxide terpolymer. *J Thermoplast Compos Mater* 2017; 30: 121–140.
19. Tekay E, Nugay N, Nugay T, et al. Revolution/rotation-type mixing-assisted masterbatch process for polypropylene-based high-impact ternary nanocomposites. *Polym Compos* 2019; 40: 24–36.
20. Tekay E, Nugay N, Nugay T, et al. Tuning of nanotube/elastomer ratio for high damping/tough and creep resistant polypropylene/SEBS-g-MA/HNT blend nanocomposites. *J Compos Mater* 2019; 53: 1005–1022.
21. He Y, Xu W, Tang R, et al. pH-Responsive nanovalves based on encapsulated halloysite for the controlled release of a corrosion inhibitor in epoxy coating. *RSC Adv* 2015; 5: 90609–90620.
22. Mercedes Pastor-Blas M. Compatibility improvement between chlorinated thermoplastic rubber and polychloroprene adhesive. *Rubber Chem Technol* 2009; 82: 18–36.
23. Pasbakhsh P, Ismail H, Fauzi MNA, et al. The partial replacement of silica or calcium carbonate by halloysite nanotubes as fillers in ethylene propylene diene monomer composites. *J Appl Polym Sci* 2009; 113: 3910–3919.
24. Ye Y, Chen H, Wu J, et al. High impact strength epoxy nanocomposites with natural nanotubes. *Polymer* 2007; 48: 6426–6433.
25. Deng S, Zhang J and Ye L. Halloysite–epoxy nanocomposites with improved particle dispersion through ball mill homogenisation and chemical treatments. *Compos Sci Technol* 2009; 69: 2497–2505.

26. Gaaz TS, Hussein EK and Al-Amiery AA. Physical properties of halloysite nanotubes-polyvinyl alcohol nanocomposites using malonic acid crosslinked. *Jurnal Kejuruteraan* 2017; 29: 71–77.
27. Yuan P, Southon PD, Liu Z, et al. Functionalization of halloysite clay nanotubes by grafting with γ-aminopropyltriethoxysilane. *J Phys Chem C* 2008; 112: 15742–15751.
28. Zhou X, Zhang Q, Wang R, et al. Preparation and performance of bio-based carboxylic elastomer/halloysite nanotubes nanocomposites with strong interfacial interaction. *Compos A Appl Sci Manuf* 2017; 102: 253–262.
29. Jamaludin NA, Inuwa IM, Hassan A, et al. Mechanical and thermal properties of SEBS-g-MA compatibilized halloysite nanotubes reinforced polyethylene terephthalate/polycarbonate/ nanocomposites. *J Appl Polym Sci* 2015; 132: 42608.
30. Bhuvana S and Prabakaran M. Synthesis and characterisation of polyamide/halloysite nanocomposites prepared by solution intercalation method. *Nanosci Nanotechnol* 2014; 4: 44–51.
31. Arat R and Uyanık N. Surface modification of nanoclays with styrene-maleic anhydride copolymers. *Nat Resour* 2017; 8: 159–171.
32. Kuester S, Merlini C, Barra GM, et al. Processing and characterization of conductive composites based on poly (styrene-b-ethylene-ran-butylene-b-styrene)(SEBS) and carbon additives: a comparative study of expanded graphite and carbon black. *Compos B Eng* 2016; 84: 236–247.
33. Rath T and Li Y. Nanocomposites based on polystyrene-b-poly (ethylene-r-butylene)-b-polystyrene and exfoliated graphite nanoplates: effect of nanoplatelet loading on morphology and mechanical properties. *Compos A Appl Sci Manuf* 2011; 42: 1995–2002.
34. Weibo H and Fengchang Z. Studies on the dynamic mechanical and vibration damping properties of polyether urethane and epoxy composites. *J Appl Polym Sci* 1993; 50: 277–283.
35. Ishak ZM, Chow W and Takeichi T. Compatibilizing effect of SEBS-g-MA on the mechanical properties of different types of OMMT filled polyamide 6/polypropylene nanocomposites. *Compos A Appl Sci Manuf* 2008; 39: 1802–1814.
36. Lecouvet B, Sclavons M, Bourbigot S, et al. Water-assisted extrusion as a novel processing route to prepare polypropylene/halloysite nanotube nanocomposites: structure and properties. *Polymer* 2011; 52: 4284–4295.
37. Liu C, Luo Y, Jia Z, et al. Enhancement of mechanical properties of poly (vinyl chloride) with polymethyl methacrylate-grafted halloysite nanotube. *Exp Polym Lett* 2011; 5: 591–603.